

Dielectric investigations of the dynamic glass transition in nanopores

M. Arndt, R. Stannarius, W. Gorbatschow, and F. Kremer
Fakultät für Physik, Universität Leipzig, 04103 Leipzig, Germany
 (Received 15 December 1995)

Broadband dielectric spectroscopy (10^{-2} Hz– 10^9 Hz) is employed to study the dynamic glass transition of low-molecular-weight glass-forming liquids being confined to nanoporous sol-gel glasses with pore sizes of 2.5, 5.0, and 7.5 nm. As glass-forming liquids, salol (one hydroxy group), pentylene glycol (two hydroxy groups), and glycerol (three hydroxy groups) were chosen. We interpret the dielectric spectra in terms of a two-state model with dynamic exchange between a bulklike phase in the pore volume and an interfacial phase close to the pore wall. This enables one to analyze in detail the interplay between the molecular dynamics in the two subsystems (bulklike and interfacial), its dynamic exchange, and hence their growth and decline in dependence on temperature and strength of the molecular interactions. For glycerol it is shown that a bulklike dynamic glass transition takes place in subvolumes as small as about 1 nm. [S1063-651X(96)08711-9]

PACS number(s): 61.25.Em, 77.22.Gm, 64.70.Pf

I. INTRODUCTION

The physics of micro- and nanoconfined systems has attracted much interest in scientific research in the past. Various types of adsorbate systems with high porosity have been investigated. In particular, the high surface to volume ratio allows a convenient investigation of gaseous and liquid phases near solid substrates [1–5]. Interaction energies, aligning properties of the surface material on the adsorbed molecules [6–8], and exchange effects [9] can be determined. The geometrical restrictions can produce interesting changes of the molecular diffusion properties [10–12]. On the other hand, the limiting pore sizes may also influence the thermodynamic properties of the confined phase. For example, one can observe the induction of thermodynamic phases [13,14], the shift of phase transition temperatures [15,16], as well as the change of the very character of phase transitions as a consequence of confinement [17,18].

The class of investigated adsorbates ranges from small inorganic molecules, such as hydrogen or water [6,10,19–23], organic aliphatic materials such as methane [11,24,25], or simple glass-forming liquids [16,26,27] to complex aromatic systems including liquid-crystal mesogens [13,14,28,29] and polymers [12,30]. Frequently used adsorbents are, for example, zeolites [24,11], silica gels and aerosil [18,28,31], aluminum oxides, hydroxides or aluminosilicates [32], and porous polymer membranes. In particular, nanoporous sol-gel glasses [33,34] have been demonstrated to be an ideal host system for studying modified liquid behavior and effects of confinement on liquids in small pores due to their chemical and mechanical stability, transparency, and huge inner surfaces. Pore sizes of these systems range from a few angstroms to a few tenths of a micrometer. Among the experimental methods, NMR (transverse and longitudinal relaxation, Overhauser effect, or line-shape analysis) [6,10,11,24,35,36], picosecond birefringence methods [37–39], differential scanning calorimetry (DSC) [15,40], neutron scattering [23,26], dynamic light scattering [12,28,30,41], Raman scattering [13,25], and dielectric spectroscopy [16,22,27] have proved particularly successful.

A challenging subject of interest is the study of the dy-

amic glass transition in confined volumes [16,26,42]. Several theories of the dynamic glass transition predict an increase in collectivity of molecular dynamics when the glass transition temperature is approached [43]. This process should manifest in the growth of cooperatively reorienting clusters of molecules [44]. It is therefore quite natural to test such theories in porous media. When glass-forming liquids are adsorbed to sol-gel glasses with a pore diameter of a few nanometers, one should expect limiting influences of the cage on the increase of cooperativity and the slowing down of dynamic processes [45]. When the cluster sizes reach the pore diameters, deviations from the bulk dynamic behavior should be observed. The temperature characteristics of molecular dynamics can provide an estimate of the cluster dimensions in the vicinity of the glass transition [46,47].

We have chosen broadband dielectric spectroscopy as a convenient tool to probe the dynamics of several glass-forming organic liquids. The materials chosen include salol as a typical van der Waals glass, hydrogen bonded pentylene glycol (PeG), and glycerol.

II. SAMPLE PREPARATION AND EXPERIMENTAL SETUP

Reagent grade pentylene glycol and salol were obtained from Aldrich Chemical Company and glycerol samples from Fluka BioChemika Company. Controlled porous glass from Geltech Inc. with specific pore sizes of 2.5, 5.0, and 7.5 nm and a narrow pore size distribution was used. The material is provided in cylindrical form (diameter 10 mm, height 10 mm). By means of a diamond string saw, the cylinders are cut into 0.2-mm-thick disk slices. Their outer surface is negligible compared to the huge inner surface ($520\text{--}610\text{ m}^2/\text{g}$).

After evacuating the porous glasses to 10^{-5} mbar at 570 K for 24 h in order to remove water and other volatile impurities, the pores were filled by capillary wetting during 48 h at a temperature of about 10 K above the melting point of the liquids. For that purpose the glass-forming liquid was injected in the (closed) vacuum chamber by means of a syringe. Both sides of the sample disks were covered with aluminum foil (thickness 800 nm) to ensure a homogenous elec-

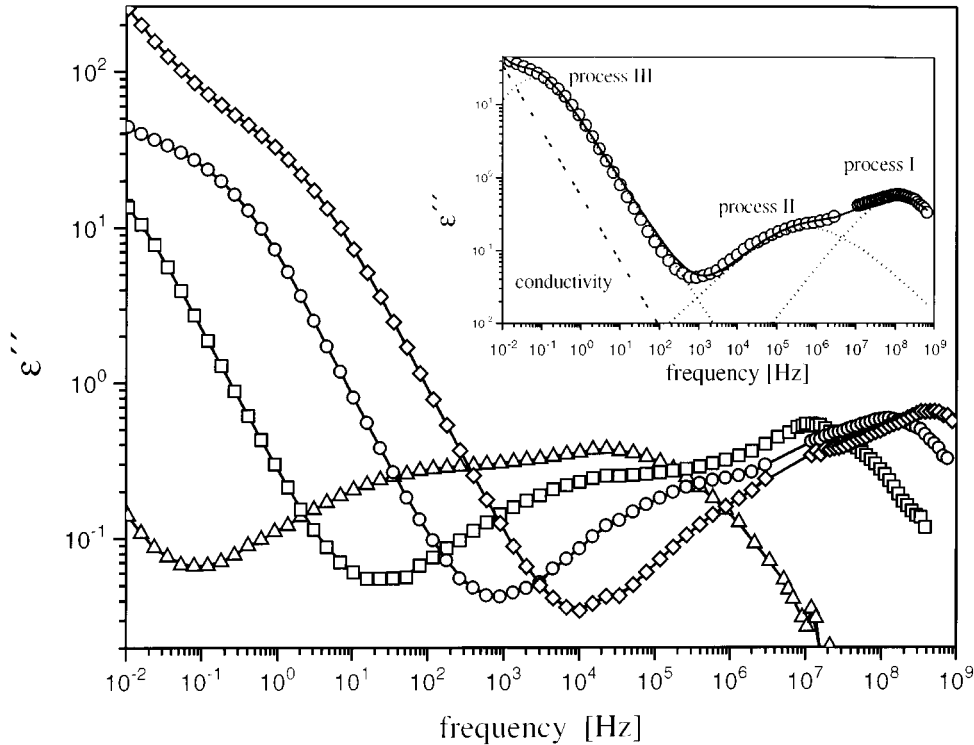


FIG. 1. Dielectric loss ϵ'' of salol in 7.5-nm pores versus frequency: \triangle , 245 K; \square , 265 K; \circ , 285 K; and \diamond , 305 K. The error of the measured data is smaller than the symbols. The inset illustrates the deconvolution of the data for $T=285$ K.

tric field distribution and were mounted between gold-plated brass electrodes of the capacitor.

Dielectric measurements in the frequency range 10^{-2} – 10^9 Hz were performed using a Solartron-Schlumberger frequency response analyzer FRA 1260 with a Novocontrol active sample cell BDC-S (10^{-2} – 3×10^6 Hz) and a Hewlett Packard impedance analyzer 4191A (10^6 – 10^9 Hz). The sample temperatures were controlled in a nitrogen gas jet with a stability better than ± 0.05 K. Details of the experimental setup may be found in Ref. [48]. DSC measurements were carried out with a Perkin-Elmer series 7 thermal analysis system.

In order to describe the dielectric spectra quantitatively, a superposition of model functions according to Havriliak and Negami [49] and a conductivity contribution have been fitted to the isothermal dielectric loss data ϵ'' :

$$\epsilon'' = \frac{\sigma_0}{\epsilon_0} \frac{1}{\omega^s} - \sum_{k=1}^3 \text{Im} \left[\frac{\Delta \epsilon_k}{[1 + (i\omega\tau_k)^{\alpha_k}]^{\beta_k}} \right]. \quad (1)$$

In this notation, ϵ_0 is the vacuum permittivity, σ_0 the dc conductivity, $\Delta \epsilon$ the dielectric strength, and τ the mean relaxation time. The index k refers to the different processes that contribute to the dielectric response. α_k and β_k describe the symmetric and asymmetric broadening of the relaxation time distribution. The first term on the right-hand side of Eq. (1) is caused by translational motion of mobile charge carriers. For Ohmic behavior, $s=1$; deviations ($s < 1$) are caused by electrode polarization.

III. EXPERIMENTAL RESULTS

We start with the description of the salol dielectric spectra, which show the most obvious differences between bulk and confined phase. Figure 1 shows the imaginary part ϵ'' of the dielectric function of the quasi van der Waals liquid salol (carrying one hydroxy group) adsorbed in 7.5-nm pores for different temperatures. The inset illustrates the deconvolution of the data: dotted lines indicate Havriliak-Negami (HN) functions, the dashed line denotes the conductivity term, and the solid line gives the superposition of all contributions. In addition to the high-frequency dynamic process (I), two further loss processes can be seen. The second process has a dielectric strength of approximately the same order of magnitude as the first, whereas the third loss process in the conductivity wing is much stronger. Qualitatively, these features can be observed for salol in all pores of the different sizes. In Fig. 2, the relaxation rate [Fig. 2(a)] and the volume corrected dielectric strength [Fig. 2(b)] of all processes of salol confined in porous glasses are plotted versus the inverse temperature. The bulk salol data are included for comparison.

The fastest process observed in the confined system obviously coincides with the relaxation curve of bulk salol at least at high temperatures, and it is therefore reasonable to attribute this process to the relaxation of bulklike salol molecules in the pore volume. The relaxation rate of the second process II is slower than that of the bulklike salol by approximately two orders of magnitude.

We assign this process to a relaxation in an interfacial layer of surface bound salol. This result is in agreement with time-resolved birefringence measurements of Warnock and

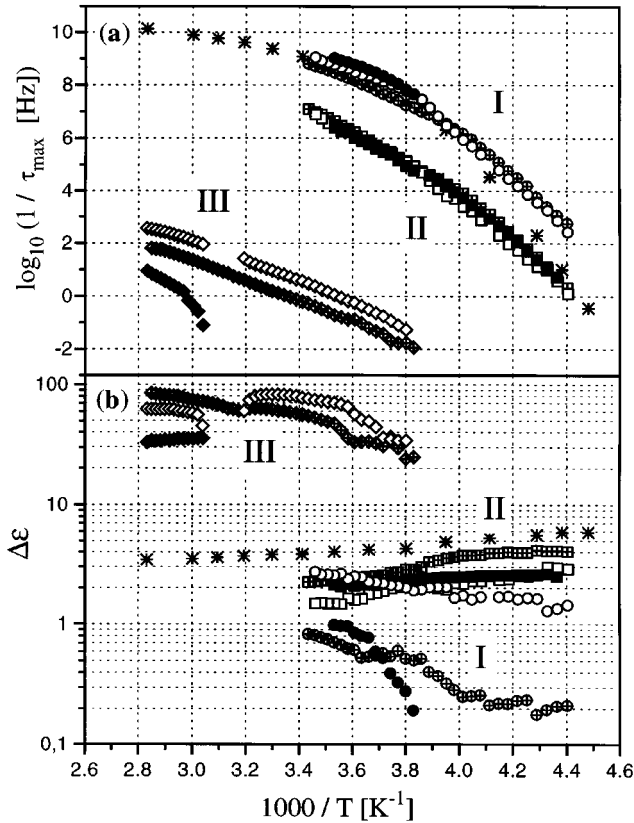


FIG. 2. (a) Decimal logarithm of the relaxation rate $1/\tau_{\max}$ and (b) volume corrected dielectric strength $\Delta\epsilon$ of salol in pores versus the inverse temperature $1000/T$. Pore sizes: 2.5 nm, solid symbols; 5.0 nm, cross-centered symbols; and 7.5 nm, open symbols. Different processes: dynamic glass transition, circles; interfacial relaxation process, boxes; and Maxwell-Wagner polarization, diamonds. Bulk salol, *.

Awshalom [50], who found an interfacial layer with a three times longer relaxation time for nitrobenzene, and NMR measurements of Liu *et al.* [7], who estimated the relaxation rate of the interfacial layer of pyridine to be about 30 times smaller than for bulk relaxation. For salol in porous glasses the interfacial process was also observed with dynamic light scattering [51]. Various theoretical studies have been performed to investigate the effect of interfaces on the relaxation of dipoles: Urbakh and Klafter [52,53] applied nonlocal screening theory to study the rotational relaxation of an interfacial dipole; major changes were found for structural changes of the liquid near a solid boundary. Benjamin [54,55,21,56] observed a significantly slower relaxation rate at a liquid-liquid interface by means of molecular-dynamics methods. Although the quantitative effects of the slowed dynamics in the interfacial layer with respect to the free molecules is obviously strongly dependent upon the very system under investigation and the surface interactions of the molecules, it is well established by experimental and theoretical work that such interfacial layers of retarded dynamics exist in confined wetting liquids. Our experiments are therefore in good agreement with these results. Because of the much higher relaxation strength of the third, very slow process as compared to the bulk, this process has to be assigned to Maxwell-Wagner polarization, i.e., the hindered motion of

TABLE I. Parameters of the VFT equations and the dielectric and calorimetric glass transition temperatures T_g^{diel} , T_g^{cal} for salol in porous glasses.

Pore size (nm)	A (fs)	D	T_0 (K)	T_g^{diel} (K)	T_g^{cal} (K)
bulk	100	4.8	194	222	222
7.5	1.8	8.0	177	215	214
5.0	170	5.3	185	214	215

free charge carriers inside the pores [57].

The relaxation rate of process I of salol in 7.5-nm and 5.0-nm pores at high temperatures is the same as in bulk salol, but with decreasing temperature the dynamics becomes faster than for bulk salol at comparable temperatures. For salol in 2.5-nm glass, the dielectric process characteristic for the dynamic glass transition is observed only at temperatures above 255 K. The temperature dependence of the dynamic glass transition can be rationalized by a VFT equation [58]

$$\frac{1}{\tau} = A \exp\left(\frac{DT_0}{T - T_0}\right), \quad (2)$$

with prefactor A , fragility parameter D , and Vogel temperature T_0 . From a VFT fit the dielectric glass transition temperature T_g^{diel} can be estimated by calculating the temperature corresponding to $1/\tau = 0.01$ Hz. Table I shows the VFT parameters T_g^{diel} and calorimetrically determined (DSC) glass transition temperature T_g^{cal} . Between the calorimetric and the dielectrically determined glass transition temperatures, agreement is found within the experimental accuracy. In 2.5-nm pores no calorimetric glass transition can be detected.

Characteristic deviations from bulk behavior are also reflected in the temperature characteristics of dielectric strength in the confined samples. The dielectric strength $\Delta\epsilon$ of all low-molecular-weight bulk liquids slightly *increase* with decreasing temperature. In contrast, for salol in the confined geometry the apparent dielectric strength of process I *decreases* with decreasing temperature [see the circles in Fig. 2(b)], while the dielectric strength of the interfacial relaxation [process II, boxes in Fig. 2(b)] increases. This effect is more pronounced in smaller pore sizes; see the disappearance of the fast relaxation process in 2.5-nm pores at temperatures below 255 K.

For comparison we describe now the qualitatively different pentylene glycol spectra. In the H-bonded liquid PeG (with two hydroxy groups), only two loss processes are observed: a Maxwell-Wagner loss process and the dynamic glass transition. An interfacial layer cannot be directly detected with dielectric spectroscopy here. We cannot exclude that it is concealed by the strong conductivity contribution, but it is at least several orders of magnitude slower (not necessarily weaker) than the bulk process. The remaining fast process is that of the bulklike PeG molecules in the pore volume. Again, the Maxwell-Wagner process is slow and its magnitude exceeds that of the intrinsic relaxation of the PeG molecules by far. Figure 3 shows the relaxation rate and the volume corrected dielectric strength of the dynamic glass transition for bulk and confined PeG. For PeG in 7.5-nm and 5.0-nm porous glasses deviations in the relaxation rate from

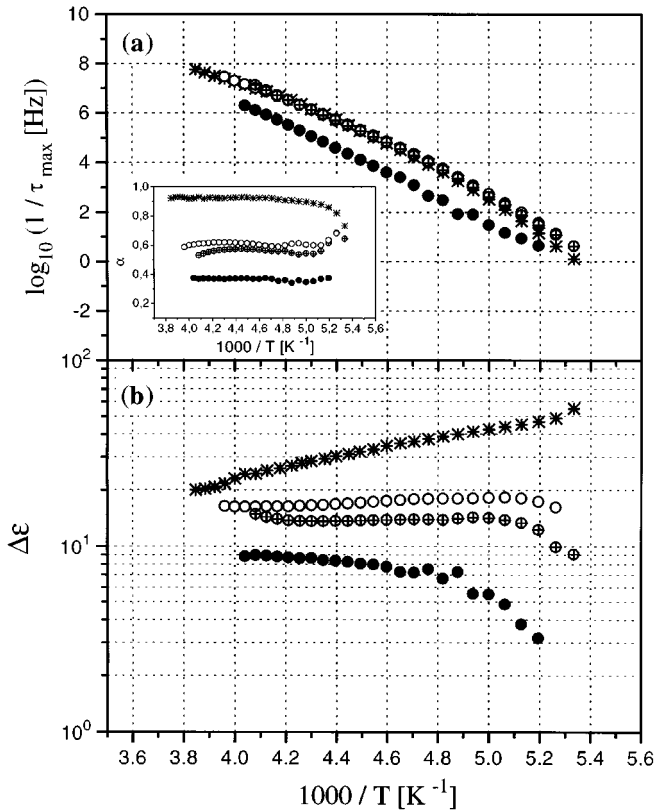


FIG. 3. (a) Decimal logarithm of the relaxation rate $1/\tau_{\max}$ and (b) volume corrected dielectric strength $\Delta\epsilon$ of the dynamic glass transition of pentylene glycol in pores versus the inverse temperature $1000/T$. Pore sizes: 2.5 nm, solid symbols; 5.0 nm, cross-centered symbols; and 7.5 nm, open symbols. Bulk pentylene glycol, *. The inset shows the broadening parameter α [see Eq. 1 with $\beta \approx 0.9$ in the whole temperature range] vs the inverse temperature.

the bulk behavior are very weak and the relaxation strength decreases at low temperatures.

In 2.5-nm pores the process connected with the dynamic glass transition is slower than the bulk relaxation at comparable temperatures over the whole temperature range. It is also broadened considerably [lower α ; compare Eq. (1)]. In the vicinity of the glass transition temperature a relative deviation of the relaxation rate curves towards faster times is indicated, connected with a decay of dielectric strength. The influences on the dielectric strength and relaxation rates are, however, much less dramatic than for salol.

Finally, for the H-bonded liquid glycerol (with three hydroxy groups) in pores two loss processes, as in PeG, are observed: the dynamic glass transition and a Maxwell-Wagner process. The relaxation rates and the volume corrected dielectric strength of the dynamic glass transition for glycerol in pores and in the bulk phase are plotted in Fig. 4. The observed relaxation rate of glycerol is the same as in the bulk for all pore sizes, even at low temperatures. The temperature dependence of the dielectric strength is comparable to bulk glycerol as well. No significant effects of molecular confinement on the relaxation rates and strength can be detected in the dielectric spectra of glycerol. However, as in the other samples investigated, the dielectric process is considerably broadened with respect to the bulk relaxation, which is reflected in a lower value of the HN parameter α .

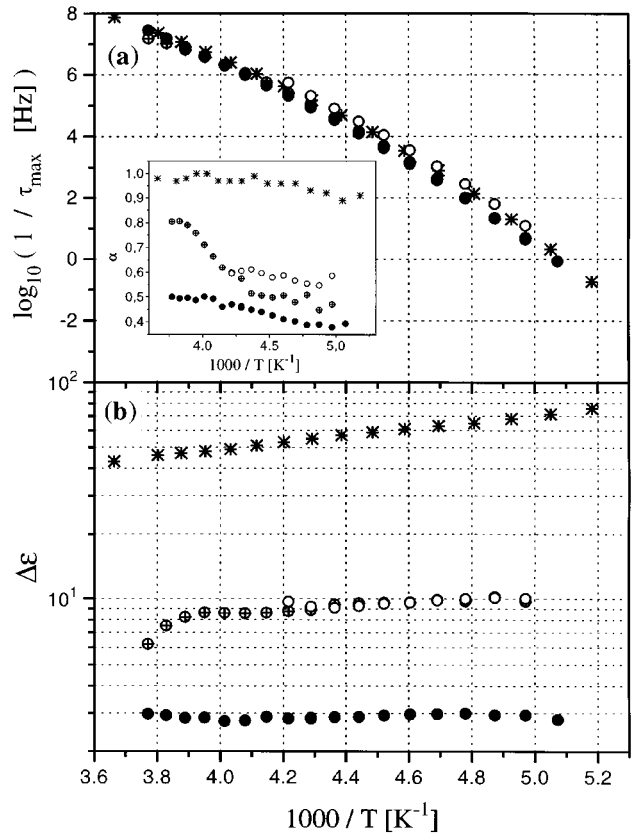


FIG. 4. (a) Decimal logarithm of the relaxation rate $1/\tau_{\max}$ and (b) volume corrected dielectric strength $\Delta\epsilon$ of the dynamic glass transition of glycerol in pores versus the inverse temperature $1000/T$. Pore sizes: 2.5 nm, solid symbols; 5.0 nm, cross-centered symbols; and 7.5 nm, open symbols. Bulk glycerol, *. The inset shows the broadening parameter α [see Eq. (1) with $\beta \approx 0.9$ in the whole temperature range] vs the inverse temperature.

IV. THEORY

In all samples investigated here, the high-frequency process coincides with the bulk relaxation dynamics at high temperatures. It is natural to assume that it originates from unbound molecules in the pore volumes. Their mobility is relatively uninfluenced by the confinement (on the time scale of the dielectric experiment) at least at high temperatures.

The existence of a well-separated second dynamic process in the spectra of salol suggests the existence of an interfacial layer with different dynamics. It is well known from the study of liquid-solid interfaces that adsorbate molecules directly attached to the substrate are strongly influenced in their reorientational dynamics, which leads to partial local ordering as well as to the slowing down of dynamic processes. In microconfined systems, the large surface-to-volume ratio leads to a considerable contribution of molecules in the interfacial layer to the dielectric spectrum (and of course to other physical properties too).

The dielectric strength of the additional dielectric process II in salol is characterized by a temperature behavior complementary to that of the fast process I. The relaxation strength of both processes sum up to a value that follows the temperature curve of the bulk relaxation strength, slightly increasing with lower temperatures. The total number of di-

electrically active salol molecules in the pores is constant; this explains why the sum of the dielectric strength of processes I and II is roughly proportional to the bulk curve. If one assumes that molecular exchange between the surface bound and unbound state is slow on the time scale of the dielectric experiment at high temperatures, the relative dielectric strength of the surface and volume processes can be taken as a direct (although not very precise) measure for the volume portions of bulklike and surface bound phases and thus for the thickness of the interfacial layer.

A comprehensive theoretical interpretation of the dielectric experiments has to explain why the interfacial process II is observed only in salol, but not in the other glass-forming liquids investigated here, and it should describe the characteristic behavior of the dielectric relaxation rates and relaxation strength in the systems with confining geometry. Several possible dynamic and geometrical effects can influence the dielectric spectra in such systems. First, the thickness of the interfacial layer can change. While it is reasonable to assume that at high temperatures only a monomolecular coverage of the pore walls with surface bound molecules exists, the thickness of this layer of interfacial molecules might increase due to cooperativity in molecular motions with lowering temperatures. The interfacial layer grows at the cost of the remaining bulklike phase in the pores. This manifests in a redistribution of the relative strength of the processes in the dielectric spectra.

Information on molecular dynamics is provided from the analysis of the relaxation frequencies. The dynamics of the interfacial and volume parts may obey different temperature characteristics. As long as the systems do not couple by exchange, the relaxation rates in the spectra directly reflect molecular dynamics in the bulklike and interfacial parts. The dielectric relaxation process in the volume does not necessarily need to be homogeneous; in larger pores or towards the pore centers, faster relaxation can be expected. The relaxation processes may be broadened due to a distribution of relaxation rates.

Finally, one has to take into account molecular exchange between the volume and interfacial subsystems on a time scale comparable to the characteristic time of the dielectric experiment. At low temperatures, in the vicinity of the glass transition, the relaxation times of both processes lower into the range of milliseconds and seconds. From this one has to consider that molecules can leave their original position and exchange between the subsystems at jump rates comparable to the relaxation rates. Such exchange processes affect the apparent relaxation rates as well as the relaxation strength of the subsystems in a theoretically predictable way.

On the basis of a quantitative analysis of all effects described above, we will construct a consistent picture of the dynamics of the adsorbed glass-forming liquids. We introduce a relatively simple shell model as depicted in Fig. 5. We treat the pores as randomly distributed elongated cylinders with axial extensions large compared to their diameters. The model is characterized by two basic quantities: the interfacial layer thickness ξ and the exchange rate c between interfacial layer and bulk. We assume for simplicity that all molecules within the free volume can be treated equivalently, i.e., that free diffusion within the pore volume is fast and a molecule inside the free pore volume visits all sites in

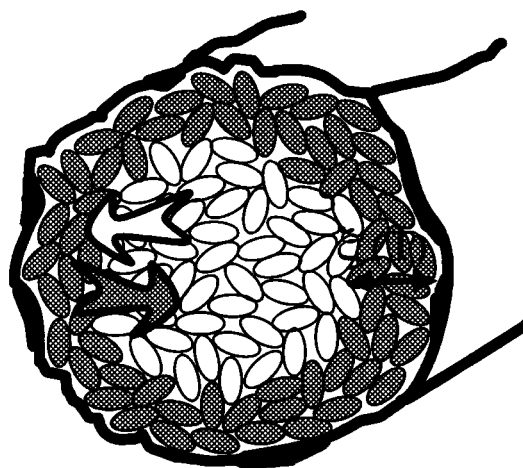


FIG. 5. Schematic view of a pore filled with glass-forming liquid. The pore walls are covered by a surface bound layer of molecules and the remaining volume is filled with bulklike molecules.

the cross section with equal probability in the time between exchange jumps. Within our model, we do not attempt to explain the physical relaxation mechanisms of interfacial molecules, i.e., we do not distinguish between molecular reorientation of bound molecules and fast desorption-readsorption processes of molecules without leaving the interfacial layer. Both effects may contribute to dielectric relaxation in state II.

We will show that most features of the experimental data can be described qualitatively by means of this simple model, which makes the straightforward assumptions that there is no effect of the confining geometry on the mobility of the bulklike molecules in the pore volumes; a layer of surface bound molecules with slower dynamics covers the pore walls and the thickness of the interfacial layer may increase with lowering temperatures; molecular exchange between interfacial and bulk molecules takes place at a time scale of milliseconds and slower, with an exchange rate that has a weaker temperature dependence than the dynamic glass transition; and with increasing number of H bonds formed by molecules attached to the surface, i.e., with increasing number of hydroxy groups per molecule, both the dynamics of the interfacial layer and the molecular exchange between interfacial layer and volume slow down considerably. Although these assumptions are rather crude, they turn out to be suited for a consistent qualitative interpretation of the dielectric spectra described above. With some reasonable additional assumptions, we are able even to give a quantitative estimate of exchange rates and interfacial layer thicknesses.

An analysis of geometry and dynamics of the model shows that the relative dielectric strength of processes I and II are determined by the interfacial layer thickness as well as by the molecular exchange. An increase of ξ lowers the strength of process I while increasing that of process II. Fast molecular exchange leads to an apparent transfer of relaxation strength in the same manner. The relaxation frequencies can be influenced by a change of the internal dynamics of states I and II, for example, a change of the glass transition temperature with respect to the bulk, and dynamic exchange may lead to apparently increased relaxation rates too.

In order to separate these effects, we present an analytical description of the two-state dynamic exchange model in the next section.

V. TWO-STATE EXCHANGE MODEL

The influence of molecular exchange in a two-state model (bulklike and interfacial molecules) on dielectric spectra has been discussed briefly in [9]. It is worthwhile to mention that the mathematical treatment given here is of course of much more general validity than for the particular system investigated in our experiment. For a universal discussion, it is convenient to refer to the well-developed theory of NMR relaxation where dynamic exchange effects have been analyzed in great detail (e.g., [59–63]). Although the underlying physical principles of dielectric and nuclear magnetic relaxation are completely different, it turns out that the predicted dynamic exchange effects are basically similar and that the respective NMR equations [60] can be easily adapted to dielectric spectra. The limits of slow and fast exchange are plainly understood. In a two-state system, one observes two distinct relaxation processes if molecular exchange between the subsystems is slow compared to the characteristic time of the experiment. When the exchange rate between two states of different relaxation characteristics crosses the sensitive time window of the experiment, critical influences on both relaxation rates are observed. If the exchange is fast compared to the characteristic time of the experiment, only one averaged relaxation rate is sensed. This fast exchange relaxation rate should be given by the averaged rates of the two original processes weighted with the relative intensities of the original processes.

It is important also to note the differences between the NMR and dielectric relaxation mechanisms, in particular the different time windows of the experiments. Dielectric polarization being the observable in dielectric spectroscopy is directly attached to the molecular orientation and the molecular dynamics immediately affects relaxation of the dielectric polarization. The relaxation rates are direct measures of the molecular reorientation dynamics. The characteristic time scale of the experiment is of the order of the molecular reorientation dynamics. The time window for the observation of exchange effects is in the range between the relaxation times of the slower and the faster process in the dielectric spectrum. The characteristic time scale can be of the order of 10^{-9} s or shorter for liquids at room temperature, whereas near the glass transition the relaxation rates slow down to less than 1 s^{-1} . Therefore, the glass transition is well suited to scan the time domain in a dielectric experiment, if one is interested in the study of surface-volume exchange processes.

In contrast, the NMR nuclear magnetization is not as directly coupled to the molecular dynamics and reorientation of molecules does not immediately lead to a reorientation of the nuclear spins. Therefore, the characteristic time for the NMR relaxation experiment is not given by the molecular reorientation times but by the NMR relaxation times T_1 or T_2 . The longitudinal relaxation time T_1 in most systems considered here is in the range of milliseconds and seconds and therefore it is usually slower than molecular exchange rates. The time window of the transverse relaxation time T_2 de-

pends upon the interactions contributing to the linewidth of the rigid lattice spectrum and can be adjusted by proper choice of the nucleus and spin interactions (dipole-dipole, chemical shift, etc.). It is usually in the range of 10^{-5} – 1 s.

We will derive now the dielectric relaxation functions of a sample with dynamic molecular exchange. Let the sample consist of two subsystems. The dielectric relaxation in each subsystem is characterized by single processes with relaxation rates $s_1 = 1/\tau_1$ and $s_2 = 1/\tau_2$, respectively. In the absence of molecular exchange between these subsystems the dielectric spectrum consists of two peaks with intensities proportional to the number of molecules in the respective subsystems. When fast molecular exchange takes place during the characteristic time of the experiment, one will observe only one averaged process that comprises the total relaxation strength of the sample.

For a description of the critical influence of dynamical exchange during the transition from the two-process to the one-process character of the dielectric spectrum, we assume two Debye processes for simplicity: $\alpha_1(t) = \exp(-s_1 t)$ and $\alpha_2(t) = \exp(-s_2 t)$ describe the relaxation functions of the molecular polarization in states 1 and 2, respectively, in the time domain when no exchange occurs. They have been normalized to $\alpha_i(0) = 1$ and can be related to the complex dielectric functions $\epsilon_i^*(\omega)$ by multiplication by a factor α_{i0} , which accounts for the respective dielectric strength (occupation number of state i) and Fourier transform of their time derivatives into the frequency domain.

We are interested in the total relaxation function $\tilde{\alpha}(t)$ of the sample polarization under exchange influence. The exact form of the exchange process is of minor significance for the effects on the dielectric spectrum; we choose a random Poisson jump process. The important parameters are the exchange rates, which determine the inverse average live times of particles in each subsystem without jump, and the relaxation rates s_i and occupation numbers n_i in the uncoupled subsystems. Two alternative, equivalent mathematical treatments can be chosen to obtain $\tilde{\alpha}(t)$.

The first, the integral equation method calculates the relaxation functions $\tilde{\alpha}_1(t), \tilde{\alpha}_2(t)$ of particles starting in states 1 and 2, respectively [normalized to $\tilde{\alpha}_{\{1,2\}}(0) = 1$]. Let the jump rates be c_{12}, c_{21} , then $c_{ij}\delta t$ is the probability that a particle changes from state i to state j during the infinitesimal time interval δt . The jump rates c_{12}, c_{21} are, in general, different and fulfill the conservation condition $c_{12}n_1 = c_{21}n_2$.

A particle in state 1 at time $t_0 = 0$ will obey the relaxation function $\alpha_1(t)$ if it performs no jumps during a time interval t . The probabilities of a particle remaining in its original state 1 or 2 are $\exp(-c_{12}t)$ or $\exp(-c_{21}t)$, respectively. If it jumps first at time $0 \leq t' \leq t$, it will be in the relaxation state $\alpha_1(t')$ at time t' and then relax with $\tilde{\alpha}_2(t-t')$ after the jump (this includes the possibility of further jumps). A first jump at time t' occurs with a probability density $c_{12}\exp(-c_{12}t')$ and $c_{21}\exp(-c_{21}t')$, respectively, for particles starting in states 1 and 2. The average relaxation function $\tilde{\alpha}_1(t)$ for particles starting in state 1 at $t=0$ is a sum of the undisturbed relaxation function multiplied by the probability that the particle remains in state 1, $\alpha_1(t)\exp(-c_{12}t)$, and of the relaxation $\alpha_1(t')\tilde{\alpha}_2(t-t')$ for particles that jump

first at time t' multiplied by the jump probability $c_{12}\exp(-c_{12}t')$ and integrated over all jump times $0 \leq t' \leq t$:

$$\tilde{\alpha}_1(t) = \alpha_1(t)e^{-c_{12}t} + \int_0^t \alpha_1(t')c_{12}e^{-c_{12}t'}\tilde{\alpha}_2(t-t')dt'. \quad (3)$$

The function $\tilde{\alpha}_2$ is calculated analogously with permutation of indices 1,2,

$$\tilde{\alpha}_2(t) = \alpha_2(t)e^{-c_{21}t} + \int_0^t \alpha_2(t')c_{21}e^{-c_{21}t'}\tilde{\alpha}_1(t-t')dt'. \quad (4)$$

We substitute $\alpha_i = \exp(-s_i t)$ and obtain a set of two coupled integral equations

$$\begin{aligned} \tilde{\alpha}_1(t) &= e^{-(s_1+c_{12})t} + c_{12} \int_0^t e^{-(s_1+c_{12})t'}\tilde{\alpha}_2(t-t')dt', \\ \tilde{\alpha}_2(t) &= e^{-(s_2+c_{21})t} + c_{21} \int_0^t e^{-(s_2+c_{21})t'}\tilde{\alpha}_1(t-t')dt'. \end{aligned}$$

Its solution can be readily found by means of a Carson-Heaviside transformation

$$p \int_0^\infty \exp(-pt)f(t)dt \equiv \mathcal{L}\{f(t)\} = \phi(p),$$

with properties

$$\mathcal{L}\{e^{-at}f(t)\} = \frac{p\phi(p+a)}{p+a}, \quad \mathcal{L}\left\{\int_0^t f(t')dt'\right\} = \frac{\phi(p)}{p}.$$

The transformed functions $\varphi_i(p) = \mathcal{L}\{\tilde{\alpha}_i(t)\}$ are related to each other by

$$\varphi_1(p) = \frac{p}{p+c_{12}+s_1} + \frac{c_{12}}{p+c_{12}+s_1}\varphi_2(p), \quad (5)$$

$$\varphi_2(p) = \frac{p}{p+c_{21}+s_2} + \frac{c_{21}}{p+c_{21}+s_2}\varphi_1(p) \quad (6)$$

and form a system of linear equations. We introduce

$$\begin{aligned} s &= \frac{s_1+s_2}{2}, & \Delta s &= \frac{s_1-s_2}{2}, \\ c &= \frac{c_{12}+c_{21}}{2}, & \Delta c &= \frac{c_{12}-c_{21}}{2}, \end{aligned}$$

$$Q^2 = c^2 + \Delta s^2 + 2\Delta s\Delta c = (c + \Delta s)^2 - 2c\Delta s \frac{2n_2}{n_1+n_2},$$

$$r = s + c,$$

where s and c are average relaxation and exchange rates, respectively, and $\Delta c/c$ can be expressed in terms of the occupation numbers $n_{\{1,2\}}$ of the subsystems by $\Delta c/c$

$= (n_2 - n_1)/(n_2 + n_1)$. After inverse transformation into the time domain, one finds the resulting normalized relaxation functions $\tilde{\alpha}_i(t)$,

$$\tilde{\alpha}_1(t) = \left(\frac{1}{2} + \frac{c - \Delta s}{2Q}\right)e^{-(r-Q)t} + \left(\frac{1}{2} - \frac{c - \Delta s}{2Q}\right)e^{-(r+Q)t}, \quad (7)$$

$$\tilde{\alpha}_2(t) = \left(\frac{1}{2} + \frac{c + \Delta s}{2Q}\right)e^{-(r-Q)t} + \left(\frac{1}{2} - \frac{c + \Delta s}{2Q}\right)e^{-(r+Q)t}. \quad (8)$$

Neither of these quantities can, however, be measured separately in the dielectric experiment, which is sensitive only to the total dielectric response of the sample. Therefore, a relevant experimental quantity is

$$\begin{aligned} \tilde{\alpha}(t) &= \frac{n_1}{n_1+n_2}\tilde{\alpha}_1(t) + \frac{n_2}{n_1+n_2}\tilde{\alpha}_2(t) \\ &= \frac{c - \Delta c}{2c}\tilde{\alpha}_1(t) + \frac{c + \Delta c}{2c}\tilde{\alpha}_2(t), \end{aligned}$$

which describes the sum of dielectric relaxation processes in the sample, normalized to $\tilde{\alpha}(0) = 1$ (we assume that the total dielectric strength of the sample is a constant that can be accounted for by a common factor, and only the relative strength of the subprocesses are of concern now). We insert Eqs. (7) and (8) and find

$$\begin{aligned} \tilde{\alpha}(t) &= \left(\frac{1}{2} + \frac{c}{2Q} + \frac{\Delta c\Delta s}{2Qc}\right)e^{-(r-Q)t} \\ &+ \left(\frac{1}{2} - \frac{c}{2Q} - \frac{\Delta c\Delta s}{2Qc}\right)e^{-(r+Q)t}. \quad (9) \end{aligned}$$

In the particular case of two equally populated subsystems, $n_1 = n_2$, $\Delta c = 0$, $c_{12} = c_{21} = c$, and $q^2 = c^2 + \Delta s^2$. Then, Eq. (9) reduces to

$$\tilde{\alpha}(t) = \left(\frac{1}{2} + \frac{c}{2q}\right)e^{-(r-q)t} + \left(\frac{1}{2} - \frac{c}{2q}\right)e^{-(r+q)t}. \quad (10)$$

A competitive mathematical approach to find this relaxation function is the solution of the rate equation. As some readers might be more acquainted with the latter approach, we will demonstrate now how the same results as above can be obtained with the solution of rate equations, and we compare both approaches. The equations describing the change of polarization $\hat{\alpha}_i$ in subsystem i form a set of coupled linear first-order differential equations if $\alpha_i(t)$ are purely exponential and the jump rate is time independent

$$\frac{d\hat{\alpha}_i}{dt} = C_{ij}\hat{\alpha}_j. \quad (11)$$

Note that $\hat{\alpha}_{\{1,2\}}$ refers to the ensemble of particles being temporarily in states 1 and 2, whereas the $\tilde{\alpha}_{\{1,2\}}$ used above describes the ensembles of particles starting in states 1 and 2, respectively.

The polarization in subsystem 1 changes by internal relaxation with the function $\alpha_1(t)$ and by transfer to and from state 2 as a consequence of jumps,

$$\frac{d\hat{\alpha}_1}{dt} = -s_1\alpha_1 - c_{12}\alpha_1 + c_{21}\alpha_2;$$

the polarization in state 2 is described analogously

$$\frac{d\hat{\alpha}_2}{dt} = -s_2\alpha_2 - c_{21}\alpha_2 + c_{12}\alpha_1$$

(the number of jumps per unit time is $c_{ij}N_i$, where N_i is the number of particles in system i , the transferred polarization for a single particle is α_i/N_i). Both equations are collected to construct the relaxation matrix

$$C_{ij} = \begin{pmatrix} -s_1 - c_{12} & c_{21} \\ c_{12} & -s_2 - c_{21} \end{pmatrix} \\ = \begin{pmatrix} -s - c - \Delta s - \Delta c & c - \Delta c \\ c + \Delta c & -s - c + \Delta s + \Delta c \end{pmatrix},$$

with eigenvalues

$$u_1 = -r + Q \quad (\text{slow process}),$$

$$u_2 = -r - Q \quad (\text{fast process}).$$

We diagonalize Eq. (11) to

$$\begin{pmatrix} \hat{\beta}_1 \\ \hat{\beta}_2 \end{pmatrix} = \begin{pmatrix} u_1 & 0 \\ 0 & u_2 \end{pmatrix} \begin{pmatrix} \beta_1 \\ \beta_2 \end{pmatrix}, \quad (12)$$

with $\beta_i = D_{ij}\hat{\alpha}_j$ and the diagonalization matrix

$$D_{ij} = \frac{1}{2Qc(c-\Delta c)} \begin{pmatrix} -\Delta s - \Delta c + Q & c - \Delta c \\ \Delta s + \Delta c + Q & -c + \Delta c \end{pmatrix},$$

$$D_{ij}^{-1} = \begin{pmatrix} c - \Delta c & c - \Delta c \\ \Delta s + \Delta c + Q & \Delta s + \Delta c - Q \end{pmatrix}.$$

The solution of Eq. (12) is

$$\beta_i = e^{u_i t} \beta_i(0) \quad \text{with } \beta_i(0) = D_{ij}\alpha_j(0).$$

Inserting $\alpha_{\{1,2\}}(0) = \frac{1}{2} \mp \frac{1}{2} \Delta c/c$ (the relative population numbers), one finds

$$\begin{pmatrix} \beta_1 \\ \beta_2 \end{pmatrix} = \frac{1}{4cq} \begin{pmatrix} (Q+c-\Delta s)e^{-(r-Q)t} \\ (Q-c+\Delta s)e^{-(r+Q)t} \end{pmatrix}, \quad (13)$$

and after transformation back to $\hat{\alpha}_i = D_{ij}^{-1}\beta_j$ we obtain the relaxation functions for states 1 and 2,

$$\hat{\alpha}_1(t) = \frac{(c-\Delta c)}{4cQ} [(Q+c-\Delta s)e^{-(r-Q)t} \\ + (Q-c+\Delta s)e^{-(r+Q)t}] \quad (14)$$

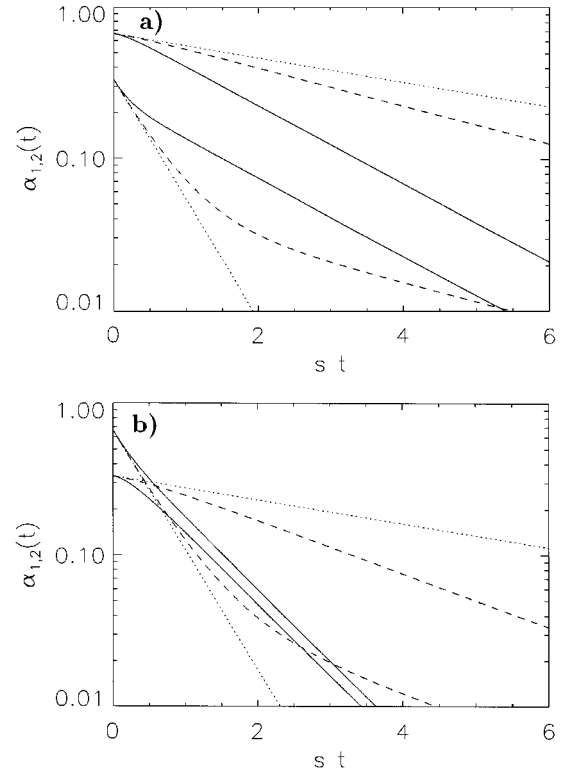


FIG. 6. Two dielectric relaxation processes under exchange presented in the time domain. The individual curves correspond to the (experimentally indistinguishable) contributions from both subsystems. The relative dielectric strengths are (a) 2:1 and (b) 1:2 for two processes with relaxation rates $s_1:s_2 = 1:10$; the average jump rates are $c=0$ (dotted line), $c=s_1$ (dashed line), and $c=s_2$ (solid line).

$$\hat{\alpha}_2(t) = \frac{(c+\Delta c)}{4cQ} [(Q+c+\Delta s)e^{-(r-Q)t} \\ + (Q-c-\Delta s)e^{-(r+Q)t}]. \quad (15)$$

Their sum is the total relaxation function of the system

$$\hat{\alpha}(t) = \tilde{\alpha}(t) = \left(\frac{1}{2} + \frac{c}{2Q} + \frac{\Delta s \Delta c}{2cQ} \right) e^{-(r-Q)t} \\ + \left(\frac{1}{2} - \frac{c}{2Q} - \frac{\Delta s \Delta c}{2cQ} \right) e^{-(r+Q)t}, \quad (16)$$

which is of course equal to the result obtained for $\tilde{\alpha}(t)$ above. Moreover, one can verify that

$$\hat{\alpha}_i(t) = \frac{n_i}{n_1+n_2} \tilde{\alpha}_i(t).$$

This means that it is equivalent whether one analyzes the relaxation of the particles starting in state i or of all particles being temporarily in state i at time t . Again, the $\hat{\alpha}_i(t)$ alone, as well as the $\tilde{\alpha}_i(t)$ given above, is not an observable in the dielectric experiment, but only their sum is a relevant quantity.

The graphs of Eqs. (14) and (15) are depicted in Fig. 6. In the limit $c_{12}=c_{21}=0$ (no exchange), the curves $\hat{\alpha}_i(t)$ coin-

cide with the original relaxation exponential functions $\hat{\alpha}_i(0)\exp(-s_i t)$. With increasing exchange rate, relaxation of the initially slow species speeds up while the faster one slows down. At no time, however, is the slope of either relaxation function under exchange steeper than that of the fast undisturbed process or slower than the undisturbed slow process. At times long compared to the jump rate, the slopes of the fast and slow process under exchange coincide, reaching the averaged relaxation rate $-s - c + Q$, which establishes an equilibrium between relaxation and polarization transfer between both subsystems. In Fig. 6(a), we have chosen a ratio $n_1/n_2=2$ of the relative intensities of both processes (faster process more intense); in Fig. 6(b), $n_1/n_2=1/2$ (the slower process is stronger).

In order to discuss the relation to dielectric spectra, we have to analyze the total relaxation function $\hat{\alpha}(t)$. As it is seen from Eqs. (10) and (16), the resulting relaxation functions can always be expressed as the sum of two exponentials. This means that any dielectric spectrum of two subsystems with intrinsic Debye relaxation coupled by dynamic exchange has the form of a superposition of two virtual Debye processes. Their apparent relaxation rates are $-s - c \pm Q$, whereas the corresponding apparent relative dielectric strength [normalized to sum 1] are

$$\frac{1}{2} \mp \left(\frac{c}{2Q} + \frac{\Delta s \Delta c}{2cQ} \right).$$

Both apparent processes become faster under the influence of dynamical exchange, and the slower process thereby gains intensity from the faster. However, none of these virtual single exponential processes can be attributed to the relaxation of a physical subsystem, as it is clearly seen from Eqs. (7), (8), (14), and (15). As soon as the relaxation processes of both subsystems couple by exchange, only their sum remains physically relevant. Therefore it is not surprising that both virtual processes apparently become faster. Such dynamic exchange effects are of course well known, for example, from the behavior of NMR longitudinal and transverse relaxation times [60], where corresponding equations can be established.

Dielectric spectroscopy is often performed in the frequency domain rather than in the time domain, therefore we have calculated the frequency dependence of the dielectric loss ϵ'' corresponding to the relaxation function of Eq. (16) in Figs. 7(a) and 7(b) for different ratios of the undisturbed slow and fast process relaxation strengths. In spite of the fact that the two individual exponential processes in Eq. (16) have no physical meaning *per se*, it is still convenient to analyze dielectric spectra as shown in this figure in terms of such simple basic functions as Debye processes even under dynamic exchange. It is evident that with a simple dielectric experiment one cannot distinguish between exchange and relaxation effects from the spectral shape. The spectra shown in Fig. 7 have the same appearance as two overlaid uncoupled Debye processes with corresponding apparent strength and relaxation rates (which are indicated by the thin lines). In view of the geometry considered in our interfacial layer model, it is particularly difficult to distinguish between fast dynamic exchange and an increase of the interfacial

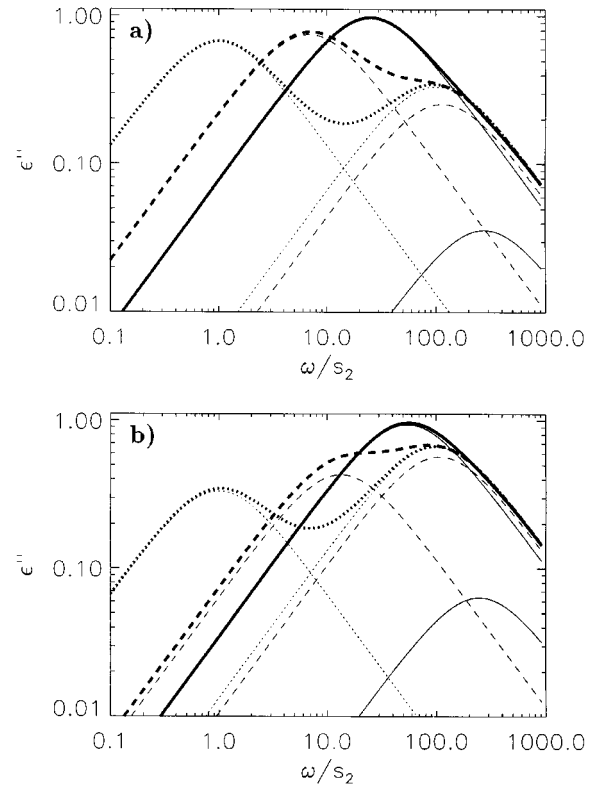


FIG. 7. Dielectric spectrum of two Debye processes under exchange ϵ'' in the frequency domain. The relative dielectric strength are (a) 2:1 and (b) 1:2, respectively, the relaxation rates are $s_1:s_2=1:100$, and the exchange rates are $c=0$ (dotted line), $c=10$ (dashed line), and $c=100$ (solid line) in units of s_1 . Thin curves depict the corresponding decomposition in single Debye curves.

layer portion from the dielectric strength and to separate a true change of the intrinsic relaxation rates from exchange effects.

A possible approach to separate dynamic exchange and intrinsic dielectric relaxation is of course the study of the temperature dependence of dielectric processes. If exchange and relaxation rates obey different temperature characteristics, they lead to a drastic change of the spectral shape with temperature. We will demonstrate here two possible scenarios. The first one is that of a VFT activated exchange rate $c(T) \propto T_c / (T - T_0)$ and of two VFT activated dielectric processes $\tau_1 = 0.01 \tau_2 \propto T_s / (T - T_0)$ with a common T_0 but different $T_c \neq T_s$ such that the temperature curve of the relaxation rates is steeper. It is depicted in Fig. 8. The horizontal axis gives a measure of the inverse temperature in arbitrary units. For comparison with the experiment, we present the apparent relaxation strength and relaxation frequencies that are influenced by the ratio c/s of exchange to relaxation rate. The dotted lines give the temperature curves of the uncoupled relaxation processes. The dashed line is the exchange rate. Again, we consider the two cases $n_1/n_2=2$ and $n_1/n_2=1/2$ and we assume that the relative occupation numbers of both subsystems (their geometrical ratios) are temperature independent.

At high temperatures where the exchange rate is low compared to both relaxation rates, one recognizes the uncoupled

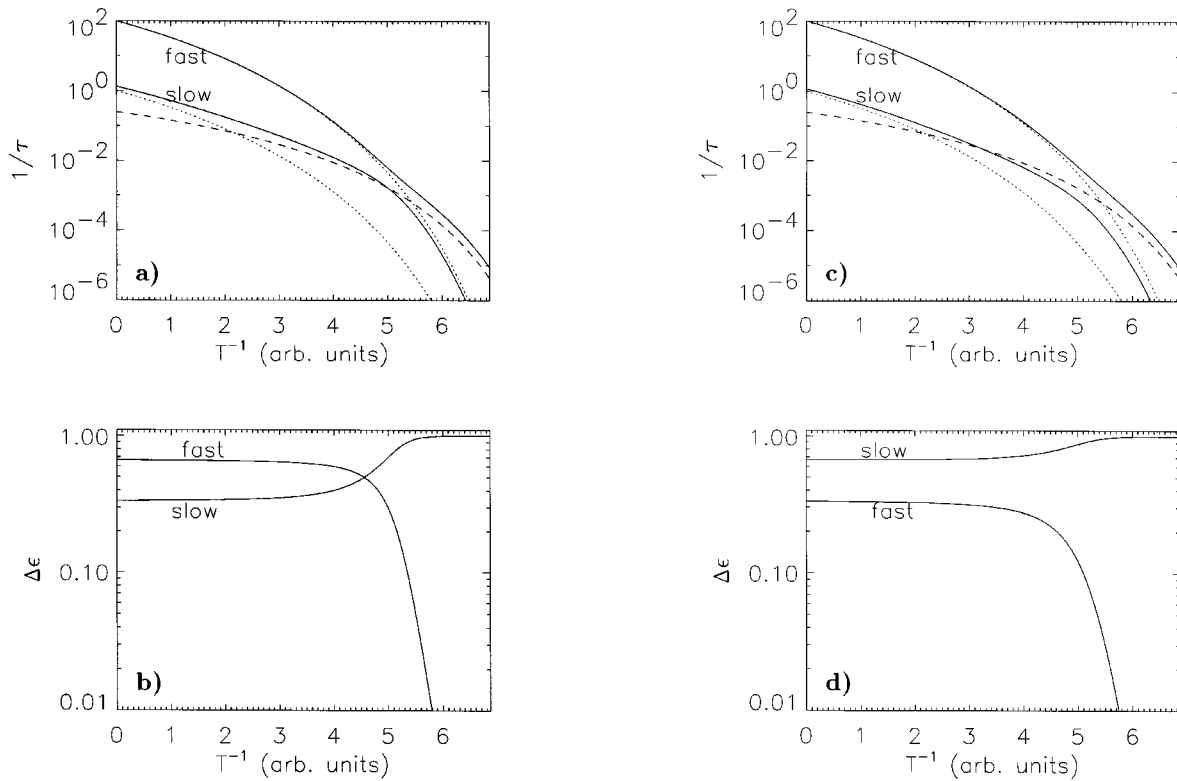


FIG. 8. Theoretical curves of the (a) and (c) apparent relaxation rates $1/\tau$ and (b) and (d) dielectric strength $\Delta\epsilon$ (b,d) with given model exchange and relaxation rates of the subsystems, where the relative volume portions are considered constant (a) and (b) 2:1 and (c) and (d) 1:2 between the fast and slow subsystems. The lines show the original fast and slow rates without exchange (dotted line), mean exchange rate c (dashed line), and apparent relaxation rates and strength (solid line). Rates are given in units of s_1 .

original processes. With lowering temperatures, the exchange becomes effective in the dielectric spectrum as c becomes comparable to the lower relaxation rate s_2 . Both individual processes are shifted to faster apparent relaxation rates. With decreasing temperature, the faster process gradually loses intensity, which is, in turn, gained by the slow process. When the exchange rate has passed the frequency window and is faster than the two undisturbed relaxation rates, only one apparent single process remains that has reached the average relaxation rate s then.

Figure 9 shows the relaxation in a system where one process does not relax intrinsically ($s_2=0$). The exchange rate is considered constant and the relaxation rate s_1 drops exponentially. Here we have chosen two equally populated subsystems. Polarization in state 2 relaxes only by exchange with state 1, hence the rate of the apparent slow process is approximately c as long as $s_1 \gg c$. When the rate of the fast process finally reaches the exchange rate, its apparent relaxation strength decays, while its apparent relaxation frequency increases with respect to the actual $s_1(T)$. The remaining slow process will no longer follow the exchange rate c but gradually adopt a rate $s = s_1/2$ and finally comprise the total dielectric strength of the two original processes.

Strictly speaking, the experimental spectra mentioned above are not composed of exact Debye processes. In the analysis of the experimental data, we have used the conventional Havriliak-Negami functions. This leads to a slight modification of the spectral appearance. A calculation of exchange effects for such nonexponential relaxation processes

is, however, very complicated and cannot be straightforwardly performed analytically. However, in an approximation one can treat such empirical functions as superpositions of Debye processes with a distribution of relaxation times. As long as these relaxation time distributions are not too broad (say, within one decade), it should still be justified to apply the above algorithm to such processes as well and to equate their relaxation strength and frequencies to the corresponding parameters of adequate Debye processes. We can therefore assume that dynamic exchange influences these rates and frequencies in the same manner as predicted for pure Debye relaxation. One can further conjecture that the processes become more Debye-like during exchange, in particular, in the fast exchange limit, because the jump processes naturally tend to average different relaxation rates of an inhomogeneous system. This is, however, beyond the scope of this paper and we will not try to analyze influences of dynamic exchange on the Havriliak-Negami parameters α_k, β_k in Eq. (1).

VI. DISCUSSION

After demonstrating the mathematical treatment of the exchange coupled two-state system, we apply the theoretical considerations to the experimental spectra that were presented above. First, we discuss the salol data. The close similarity of Figs. 2 and 8 suggests that the effects in the experimental spectra can be described by the two-state dynamic exchange model and that with a proper assignment of

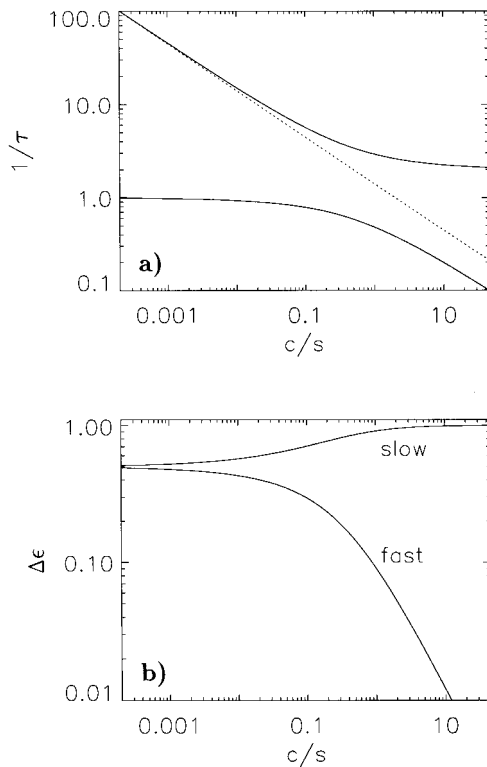


FIG. 9. Same presentation as Figs. 8(a) and 8(b), but one state is considered rigid (no dielectric relaxation), the exchange rate is assumed constant $c=1$, and only the rate of the fast process (dots) is lowered from left to right. We have chosen equally populated subsystems $n_1=n_2$.

the dielectric processes, one can extract relaxation and exchange rates as well as relative volume portions of the slow interfacial layer from the available experimental data.

The fast process that coincides with the bulk curve at high temperatures gradually loses dielectric strength to the lower-frequency process, which is obviously the interfacial layer dielectric relaxation. Their relaxation time ratio measured at high temperatures is approximately 1:140. If one considers Eq. (16) and the graphs of Figs. 8 and 9, one has to conclude that the relaxation of interfacial salol is at least two orders of magnitude slower than the bulk relaxation, but that the spectra are also compatible with a rigidly interfacial layer that relaxes only via exchange with the free volume, state I. In that case, the apparent rate of process II would be that of the dynamic exchange. We cannot decide from the dielectric spectra whether relaxation occurs at the surface or via molecular exchange between the surface layer and free pore volume. It is also possible that the major effect for relaxation of the interfacial molecules is exchange alone and that a direct dielectric relaxation via orientational dynamics at the surface may be neglected. However, such an assumption is irrelevant for the following considerations.

At high temperatures, the relaxation strength of both processes gives information on the number of molecules in the free volume and interfacial layer, respectively. If a monomolecular interfacial layer of 0.5 nm is assumed at the walls for each pore size and the pores are assumed cylinderlike, the volume ratios are approximately 3:1, 2:1, and 1:2 between the volume and interfacial parts for 7.5, 5.0, and 2.5 nm,

respectively. These ratios are relatively well reflected in the high-temperature ratios of the dielectric strength of processes I and II for the 7.5- and 2.5-nm samples, the 5.0-nm sample makes an exception.

We have shown above that dynamic exchange processes can redistribute the relative strength of the apparent single processes that are used to describe dielectric relaxation. As long as the fast relaxation rate roughly follows the bulk curve, we may assume that exchange is slower than relaxation in the free volume and that the relative relaxation strength measured will reflect basically the volume portions of interfacial layer and free pore volume.

At low temperatures, as the samples approach the glass transition temperature, dielectric relaxation rates lower to the milliseconds range. There, a pronounced deviation of process I from the bulk relaxation rate is found for the 5.0-nm and 7.5-nm samples, and we attribute this deviation to effects of molecular exchange between interfacial and free volume. Therefore, the change of the relative strength at lower temperatures is no longer an unambiguous measure for the occupation numbers of the subsystems (i.e., the interfacial layer thickness). Note that also in this case the sum of the dielectric strength of process I and II equals approximately the bulk dielectric strength. It turns out that molecular exchange alone with the assumption of an interfacial layer of constant thickness can only describe the shift of relaxation rates; the exchange rate can be equated in approximation to the measured relaxation rate of process II, but it cannot describe satisfactorily the change in dielectric strength. Growth of the interfacial layer and dynamic exchange both influence the apparent relaxation strength here. We do not attempt a quantitative analysis, but it seems, however, that for salol in 2.5-nm pores at $1000/T \text{ K}^{-1} \approx 3.9$ and roughly at $1000/T \text{ K}^{-1} \approx 4.3$ for salol in the 5.0-nm pores the pore is completely filled by the interfacial layer so its thickness approximately reaches half the size of the pores, causing the fast process to disappear in the respective samples.

The PeG spectra are characterized by a single fast process (dynamic glass transition); at high temperatures this process behaves in 7.5-nm and 5.0-nm pores exactly like the bulk relaxation. In 2.5-nm pores it is shifted to lower frequencies in the whole temperature range. We do not see an additional dielectric loss process of an interfacial layer relaxation. Therefore, we can analyze the temperature-dependent dynamic glass transition only. A significant deviation of the dielectric relaxation rate from the VFT curve towards faster relaxation is observed only for PeG in 2.5-nm pores. However, the high-frequency shift of the relaxation rate as characteristic of exchange effects is very weak. It is not suited for a discussion of relaxation rates. One can guess the magnitude of an exchange rate that would cause such an effect. The apparent fast relaxation rate speeds up and the dielectric strength decreases when the exchange rate approaches the relaxation rate. As this process sets in at about $s_{\text{fast}} = 10^3 \text{ Hz}$, we conclude that exchange rates are on the order of milliseconds or seconds, one or two orders of magnitude below s_{fast} .

In the vicinity of the glass transition temperature, we observe a decrease of the dielectric strength in all pore sizes, which is more pronounced the smaller the pore size is. The collapsing dielectric strength of the fast process at low tem-

peratures is caused by the increasing effective thickness of the interfacial layer, corresponding to a decreasing free volume portion. However, the fast process does not vanish completely; only in 2.5-nm pores does it come close to that limit. That is, the effective interfacial layer thickness remains smaller than the radius of the 2.5-nm pores.

It is characteristic, and consistent with our interpretation, that for the 2.5-nm samples the loss of intensity sets in at higher temperatures than for larger pore samples. The influence of an increasing interfacial layer thickness must be more pronounced in small pores. This result agrees well with measurements on glycols (two hydroxy groups) with different molecular volume, in which the effects of dynamic exchange become observable at higher temperatures with increasing size of the molecule [64]. These features also give evidence for a growth of the interfacial layer thickness and for exchange effects between the bulklike molecules and the interfacial layer with exchange rates in the range of milliseconds and seconds. The relaxation of the interfacial layer itself is not detected directly in the dielectric spectra.

As in PeG we observe one dielectric relaxation process for glycerol that can be assigned to bulklike molecules within the cavities (dynamic glass transition). Its dielectric relaxation rate follows strictly the temperature curve of the bulk liquid down to relaxation rates of 1 s^{-1} ; no particular systematic shift to lower frequencies is observed for glycerol in 2.5-nm pores. The significantly lowered dielectric strength compared to bulk glycerol gives evidence for the existence of an interfacial layer. But in contrast to PeG, the dielectric strength does not decrease with decreasing temperatures even at temperatures in the vicinity of the glass transition temperature.

The relaxation of the interfacial layer is not detected directly (as an additional peak in the spectra), nor do we observe any effect of a dynamic exchange of bulklike glycerol with the interfacial layer. We conclude that the interfacial layer, which is presumably present, is tightly bound to the pore walls by hydrogen bonds (three hydroxy groups per molecule). The interfacial molecules have very slow dynamics and very slow exchange rates, so their dielectric relaxation is very slow and hidden by the low-frequency conductivity and Maxwell-Wagner contributions. The thickness of the interfacial layer can be estimated from the ratio of dielectric strength in the bulk and in pores. An effective pore size of 0.7 nm is found for the 2.5-nm pores. This means that the relaxation of the bulklike molecules in the pores takes place in such a small subvolume on the same time scale like in the bulk.

The measurements of molecules with one, two, or three hydroxy groups show a systematic dependence of the dynamic behavior monitored by dielectric spectroscopy from the number of hydroxy groups. Salol molecules with only one hydrogen bond per molecule stick to the pore walls relatively loose. A relaxation of the interfacial layer can be directly observed in the dielectric spectra as an additional peak, so effects of dynamic exchange can be studied in the temperature dependence of the relaxation rate and the dielectric strength in detail. [This explanation is backed by the experimental result that a separate interfacial layer relaxation process is found also in iso-propanol (with one OH group) confined to porous glass [65].] The thickness of the interfacial

layer increases with decreasing temperature accompanied by the vanishing of the dielectric strength of the dynamic glass transition (bulklike molecules) at low temperatures. The two hydroxy groups per molecule of PeG cause a more rigid coupling of the PeG molecule to the surface. A relaxation process of the interfacial layer is not detected directly, but effects of a dynamic exchange are observed in a significant decline of the dielectric strength combined with a small deviation from the bulk relaxation rate at low temperatures. The increase of the thickness of the surface layer seems to be less pronounced compared to salol, but one has to take into account the much larger molecular volume of salol. Glycerol with three hydroxy groups per molecule should have the strongest coupling to the surface of the glass. Neither the dynamics of the interfacial layer is detected directly nor any effects of dynamic exchange are observed. The interfacial layer thickness is constant in the whole temperature range.

VII. SUMMARY AND CONCLUSIONS

We presented broadband dielectric spectra (10^{-2} – 10^9 Hz) measured on glass-forming liquids with a different number of hydroxy groups per molecule confined to nanoporous glasses with pore sizes of 2.5, 5.0, and 7.5 nm. For a liquid with one hydroxy group (salol) two separated loss processes are detected in all pore sizes that are assigned to the relaxation of an interfacial layer and the relaxation of bulklike molecules in the center of the pores (dynamic glass transition). Liquids with two (pentylene glycol) or three (glycerol) hydroxy groups exhibit only the relaxation process connected to the dynamic glass transition. In all samples an additional loss process caused by a Maxwell-Wagner polarization is observed at low frequencies. The observed spectra can be consistently interpreted within a shell model of a bulklike phase and an interfacial layer including molecular exchange between both subsystems.

From the dielectric spectra the exchange rate between the interfacial layer and the bulklike molecules can be directly deduced. For salol (one hydroxy group) the exchange can be observed already at a temperature of 70 K above the calorimetric glass transition temperature, with an exchange rate as high as 10^3 Hz. For pentylene glycol (having two hydroxy groups) exchange occurs at 30 K above T_g in the millisecond range. For glycerol (having three hydroxy groups) the exchange must be slower than 1 Hz even at temperatures of 5 K above T_g .

In parallel, the thickness of the interfacial layer increases strongly with increasing strength of the molecular interaction (number of hydroxy groups). For salol and pentylene glycol the thickness of the interfacial layer is roughly monomolecular at high temperatures and grows with decreasing temperature, but for pentylene glycol the growth of the layer thickness is less pronounced. The interfacial layer of glycerol, as estimated from the dielectric strength in 2.5-nm pores, has a thickness of about 0.9 nm. It is temperature independent in the whole temperature range. We do not detect exchange in this temperature regime.

The relaxation rate of the dynamic glass transition of con-

fined glycerol does not show a pore size dependence (diameter ≥ 2.5 nm) and it is, within the experimental accuracy, identical to the bulk. The temperature dependence of its dielectric strength is comparable to the bulk. Considering the fact that the interfacial layer has a thickness of about 0.9 nm in the smallest pores, one has to conclude that the dynamic glass transition takes place in a subvolume with a diameter of roughly 0.7 nm on a time scale as in the bulk. This is in pronounced contrast to theories of the dynamic glass transition that are based on the existence of so-called cooperatively rearranging regions, of 3–5 nm size close to the calorimetric glass transition temperature.

A more elaborate model of the systems investigated has to consider that molecular mobility increases gradually with the distance from the pore walls and the model of an effective interfacial layer is only a first approximation. However, the

fact that there is a difference of at least two decades between the observed volume and surface processes (see Fig. 2) makes the simplifications of our model quite reasonable, and any extension to more complex models will certainly improve the quantitative description but not invalidate any of the conclusions described above. Accompanying NMR experiments are being performed in our laboratory to confirm these results.

ACKNOWLEDGMENTS

The authors are indebted to E. Hempel for the DSC measurements on salol and to the DFG for financial support within the Sonderforschungsbereich SFB 294. One of us (W.G.) gratefully acknowledges support from the DAAD.

-
- [1] *Molecular Dynamics in Restricted Geometries*, edited by J. Klafter and J. M. Drake (Wiley, New York, 1989).
- [2] *Dynamics in Disordered Materials*, edited by D. Richter, A. J. Dianoux, W. Petry, and J. Teixeira, Springer Proceedings in Physics Vol. 38 (Springer, Berlin, 1989).
- [3] *Relaxation in Complex Systems*, edited by K. L. Ngai and G. B. Wright (North-Holland, Amsterdam, 1991).
- [4] *Dynamics in Small Confining Systems*, edited by J. M. Drake, J. Klafter, R. Kopelman, and D. D. Awschalom, MRS Symposia Proceedings No. 290 (Materials Research Society, Pittsburgh, 1993).
- [5] *Dynamics in Small Confining Systems*, edited by J. M. Drake, S. M. Troian, J. Klafter, and R. Kopelman, MRS Symposia Proceedings No. 366 (Materials Research Society, Pittsburgh, 1995).
- [6] S. Stapf, R. Kimmich, and R.-O. Seitter, *Phys. Rev. Lett.* **75**, 2855 (1995).
- [7] G. Liu, Y. Li, and J. Jonas, *J. Chem. Phys.* **95**, 6892 (1991).
- [8] G. P. Crawford, R. Stannarius, and J. W. Doane, *Phys. Rev. A* **44**, 2558 (1991).
- [9] R. Stannarius, F. Kremer, and M. Arndt, *Phys. Rev. Lett.* **75**, 4698 (1995).
- [10] M. D. Hurlimann, K. G. Helmer, T. M. de Swiet, P. N. Sen, and C. H. Sotak, *J. Mag. Res. A* **113**, 260 (1995).
- [11] S. Fritsche, R. Haberlandt, J. Kärger, and H. Pfeifer, *Chem. Phys. Lett.* **242**, 361 (1995).
- [12] G. Yihong, K. H. Langley, and F. E. Karasz, *Phys. Rev. B* **50**, 3400 (1994).
- [13] Y. Shao, G. Hoang, and T. W. Zerda, *J. Non-Cryst. Solids* **182**, 309 (1995).
- [14] G. Schwalb and F. W. Deeg, *Phys. Rev. Lett.* **77**, 1383 (1995).
- [15] C. L. Jackson and G. B. McKenna, *J. Chem. Phys.* **93**, 9002 (1990).
- [16] J. Schüller, Yu. Mel'nichenko, R. Richert, and E. W. Fischer, *Phys. Rev. Lett.* **73**, 2224 (1994).
- [17] B. F. Borisov, E. V. Charnaya, Yu. A. Kumzerov, A. K. Radzhabov, and A. V. Shelyapin, *Solid State Commun.* **92**, 531 (1994).
- [18] A. P. Y. Won, S. B. Kim, W. I. Goldberg, and M. H. W. Chan, *Phys. Rev. Lett.* **70**, 954 (1993).
- [19] M.-C. Bellissent-Funel, S. H. Chen, and J.-M. Zanotti, *Phys. Rev. E* **51**, 4558 (1995).
- [20] M. J. Benham, J. C. Cook, J.-C. Li, D. K. Ross, P. L. Hall, and B. Sarkissian, *Phys. Rev. B* **39**, 633 (1989).
- [21] I. Benjamin, *J. Chem. Phys.* **90**, 7535 (1989).
- [22] D. Daoukaki-Diamanti and P. Pissis, in *Proceedings of the Seventh International Symposium on Electrets*, edited by R. Gerhard-Mulhaupt, W. Kunstler, L. Brehmer, and R. Danz (IEEE, New York, 1991).
- [23] J.-C. Li, D. K. Ross, and M. J. Benham, *J. Appl. Cryst.* **24**, 794 (1991).
- [24] S. Brandani, D. M. Ruthven, and J. Kärger, *Zeolites* **15**, 494 (1995).
- [25] L. Nikiel, B. Hopkins, and T. W. Zerda, *J. Chem. Phys.* **94**, 7458 (1990).
- [26] Yu. Mel'nichenko, J. Schüller, R. Richert, B. Ewen, and C.-K. Loong, *J. Chem. Phys.* **103**, 2016 (1995).
- [27] M. Arndt and F. Kremer, in *Dynamics in Small Confining Systems* (Ref. [5]), p. 259.
- [28] T. Bellini, N. A. Clark, and D. W. Schaefer, *Phys. Rev. Lett.* **74**, 2740 (1995).
- [29] S. Tripathi, C. Rosenblatt, and F. M. Aliev, *Phys. Rev. Lett.* **72**, 2725 (1994).
- [30] Y. Guo, K. H. Langley, and F. E. Karasz, *J. Chem. Phys.* **93**, 7457 (1990).
- [31] S. Tschierske, O. V. Yaroshchuk, and H. Kresse, *Cryst. Res. Tech.* **30**, 571 (1995).
- [32] Y. Weijun, J. Tanaka, and D. H. Damon, *IEEE Trans. Dielectr. Electr. Insul.* **1**, 169 (1994).
- [33] M. W. Shafer, D. D. Awshalom, and J. Warnock, *J. Appl. Phys.* **61**, 5438 (1987).
- [34] I. Tilgner, P. Fischer, F. M. Bohnen, H. Rehage, and W. F. Maier, *Microporous Mater.* **5**, 77 (1995).
- [35] H. Pfeifer, *NMR—Basic Principles Prog.* **31**, 31 (1994).
- [36] J. Kärger and D. M. Ruthven, *Diffusion in Zeolites* (Wiley, New York, 1992).
- [37] J. Warnock, D. D. Awshalom, and M. W. Shafer, *Phys. Rev. Lett.* **57**, 1753 (1986).
- [38] D. D. Awshalom and J. Warnock, *Phys. Rev. B* **35**, 6779 (1987).

- [39] M. B. Ritter, D. D. Awshalom, and M. W. Shafer, *Phys. Rev. Lett.* **61**, 966 (1988).
- [40] V. M. Buleiko, V. P. Voronov, L. V. Entow, and A. R. Ramanow, *Pis'ma Zh. Éksp. Teor. Fiz.* **61**, 34 (1995) [*JETP Lett.* **61**, 34 (1995)].
- [41] N. Ostrowsky and L. Lobry, *Nuovo Cimento D* **16**, 1111 (1994).
- [42] P. Pissis, D. Daoukakis-Diamanti, L. Apekis, and C. Christodoulides, *J. Phys.* **6**, L325 (1994).
- [43] G. Adam and J. H. Gibbs, *J. Chem. Phys.* **43**, 139 (1965).
- [44] E. Donth, *J. Non-Cryst. Solids* **131-133**, 204 (1991).
- [45] D. Sappelt and J. Jäckle, *J. Phys. A* **26**, 7325 (1993).
- [46] E. W. Fischer, E. Donth, and W. Steffen, *Phys. Rev. Lett.* **68**, 2344 (1992).
- [47] G. Katana, E. W. Fischer, Th. Hack, V. Abetz, and F. Kremer, *Macromolecules* **28**, 2714 (1995).
- [48] F. Kremer, D. Boese, G. Maier, and E. W. Fischer, *Prog. Polym. Sci.* **80**, 129 (1989).
- [49] S. Havriliak and S. Negami, *J. Polym. Sci. C* **14**, 99 (1966); *Polymer* **8**, 161 (1967).
- [50] J. Warnock and D. D. Awshalom, *Phys. Rev. B* **34**, 475 (1986).
- [51] A. Patkowski (private communication).
- [52] M. Urbakh and J. Klafter, *J. Phys. Chem.* **96**, 3480 (1992).
- [53] M. Urbakh and J. Klafter, in *Disorder Effects on Relaxational Processes*, edited by R. Richert and A. Blumen (Springer, Berlin, 1993), p. 279.
- [54] D. A. Rose and I. Benjamin, *J. Chem. Phys.* **102**, 5292 (1995).
- [55] I. Benjamin, *Phys. Rev. Lett.* **73**, 2803 (1994).
- [56] I. Benjamin, *Chem. Phys.* **180**, 287 (1994).
- [57] K. W. Wagner, *Arch. Elektrotech.* **2**, 378 (1914).
- [58] H. Vogel, *Phys. Z.* **22**, 645 (1921); G. S. Fulcher, *J. Am. Chem. Soc.* **8**, 339 (1925).
- [59] J. R. Zimmermann and W. E. Brittin, *J. Phys. Chem.* **61**, 1328 (1957).
- [60] D. E. Woessner, *J. Chem. Phys.* **35**, 41 (1961).
- [61] J. E. Anderson and R. Ullmann, *J. Chem. Phys.* **47**, 2178 (1967).
- [62] H. Sillescu, *J. Chem. Phys.* **54**, 2110 (1971).
- [63] H. Pfeifer, *NMR—Basic Principles Prog.* **7**, 55 (1972).
- [64] W. Gorbatschow, M. Arndt, R. Stannarius, and F. Kremer *Europhys. Lett.* (to be published).
- [65] M. Arndt (unpublished).